Joint target-oriented wave-equation inversion of multiple time-lapse seismic data sets

Gboyega Ayeni and Biondo Biondi, Stanford University*

SUMMARY

We propose a joint target-oriented wave-equation inversion method for multiple time-lapse seismic data sets. Complex reservoir overburden or acquisition geometry difference degrade the quality of time-lapse seismic images. This degradation occurs because the imaging operator does not account for overburden and geometry artifacts. Under such conditions, time-lapse images are poor indicators of production-related changes in reservoir properties. To solve this problem, we pose time-lapse imaging as a joint linear inverse problem that utilize concatenations of target-oriented approximations to the least-squares imaging Hessian. The proposed method outputs a baseline image and time-lapse images from multiple seismic data sets. Using a 2D synthetic sub-salt model, we show that this method attenuates overburden and geometry artifacts and that it gives reliable time-lapse seismic images.

INTRODUCTION

There is a wide range of published work on the most important aspects of time-lapse seismic imaging. Some of these include rock and fluid relationships (Batzle and Wang, 1992), processing and practical applications (Rickett and Lumley, 2001; Calvert, 2005), and successful case studies (Lefeuvre et al., 2003; Whitcombe et al., 2004; Zou et al., 2006). Because of many successful applications, time-lapse seismic imaging is now an integral part of many reservoir management projects.

Many *conventional* time-lapse seismic processing methods are adequate in fairly simple geology— where, for example, time-migration methods sufficiently image the targets. However, hydrocarbon exploration and production have shifted from geologically simple to complex environments (e.g., sub-salt reservoirs) where conventional time-lapse processing methods are inadequate. For example, conventional methods are inadequate to correct for poor and uneven illumination. Many conventional methods are also usually unable to perfectly reconcile large differences in the acquisition geometries between surveys. Such large geometry differences can be caused by changes acquisition methods, production facilities (not present during baseline data acquisition), or natural environmental changes (e.g., strong ocean currents). Unless seismic data sets are matched, non-production-related artifacts make it is impossible to accurately relate time-lapse seismic images to changes in reservoir properties. Because of limitations in conventional methods, new time-lapse imaging methods are needed.

We propose a joint target-oriented inversion method based on a linearized approximation to the acoustic wave-equation. The method utilizes a system of non-stationary filters derived from explicitly computed target-oriented approximation (Valenciano, 2008) to the linear least-squares wave-equation Hessian. A joint inversion scheme enables incorporation of prior knowledge of the reservoir location, extent and geometry together with temporal constraints in the estimation of the time-lapse seismic images. We call the proposed method *regularized joint inversion for image differences* (RJID) because it outputs a single inverted baseline image and time-lapse seismic image differences.

We assume that the background baseline velocity model is known and that it changes slowly between surveys. Large velocity changes and geomechanical shifts can be handled by including an event alignment step prior to or during inversion. Although we do not directly invert for actual reservoir property changes, such properties can be estimated from the recovered time-lapse seismic images. Integration of geomechanical shifts into RJID is ongoing and will be discussed elsewhere.

In this paper, we first review linear wave-equation modeling, least-squares migration/inversion and the RJID method. Then, using a 2D synthetic sub-salt reservoir example, we show that RJID corrects for geometry differences and uneven illumination and that it gives better results than migration and *separate inversion*.

LINEAR LEAST-SQUARES MODELING/INVERSION

From the Born approximation of the linearized acoustic wave equation, the synthetic seismic data d^s recorded by a receiver at $\mathbf{x_r}$ due to a shot at $\mathbf{x_s}$ is given by

$$d^s(\mathbf{x_s},\mathbf{x_r},\omega) = \omega^2 \sum_{\mathbf{x}} f_s(\omega) G(\mathbf{x_s},\mathbf{x},\omega) G(\mathbf{x},\mathbf{x_r},\omega)\mathbf{m}(\mathbf{x}), \quad (1)$$

where ω is frequency, $\mathbf{m}(\mathbf{x})$ is *reflectivity* at image points $\mathbf{x}$, $f_s(\omega)$ is source waveform, and $G(\mathbf{x_s},\mathbf{x},\omega)$ and $G(\mathbf{x},\mathbf{x_r},\omega)$ are Green's functions from $\mathbf{x_s}$ to $\mathbf{x}$ and from $\mathbf{x}$ to $\mathbf{x_r}$ respectively.

Taking the true recorded data at $\mathbf{x_r}$ to be d^t, the quadratic cost function is given by

$$S(\mathbf{m}) = \|d^s(\mathbf{x_s},\mathbf{x_r},\omega) - d^t(\mathbf{x_s},\mathbf{x_r},\omega)\|_2^2. \quad (2)$$

As shown by previous authors (Plessix and Mulder, 2004; Valenciano, 2008), the gradient $g(x)$ of this cost function with respect to reflectivity (summed over sources and receivers) is

$$g(\mathbf{x}) = \sum_w \omega^2 \sum_{\mathbf{x_s}} \sum_{\mathbf{x_r}} f_s(\omega) G(\mathbf{x_s},\mathbf{x},\omega) G(\mathbf{x},\mathbf{x_r},\omega) \left(d^s - d^t\right), \quad (3)$$

and the Hessian (second derivatives) is

$$H\left(\mathbf{x},\mathbf{x}'\right) = \sum_w \omega^4 \sum_{\mathbf{x_s}} |f(s)|^2 G(\mathbf{x_s},\mathbf{x},\omega)\bar{G}(\mathbf{x_s},\mathbf{x}',\omega) \sum_{\mathbf{x_r}} G(\mathbf{x},\mathbf{x_r},\omega)\bar{G}(\mathbf{x}',\mathbf{x_r},\omega), \quad (4)$$

where $\mathbf{x}'$ denotes all image points and $\bar{G}$ is the complex conjugate of G. Plessix and Mulder (2004) and Valenciano (2008) discuss this derivation in detail.

Target-oriented Hessian

The large computational cost of full Hessian (equation 4) makes explicit computation impractical. Previous authors (Shin et al., 2001; Rickett, 2003; Guitton, 2004; Plessix and Mulder, 2004; Valenciano, 2008; Symes, 2008) have discussed possible approximations that reduce the computational cost or remove the need for explicit computation of the full Hessian.

Because reservoirs are limited in extent, the region of interest is usually smaller than the full image space, therefore, the Hessian can be explicitly computed for that region. For our problem, we follow the target-oriented approximation (Valenciano, 2008) to the Hessian, which for a target region $\mathbf{x_T}$ is

$$H(\mathbf{x_T},\mathbf{x_{T+a_x}}) = \sum_w \omega^4 \sum_{\mathbf{x_s}} |f(s)|^2 G(\mathbf{x_s},\mathbf{x_T},\omega)\bar{G}(\mathbf{x_s},\mathbf{x_{T+a_x}},\omega) \sum_{\mathbf{x_r}} G(\mathbf{x_T},\mathbf{x_r},\omega)\bar{G}(\mathbf{x_{T+a_x}},\mathbf{x_r},\omega), \quad (5)$$

where $\mathbf{x_{T+a_x}}$ represents a *small* region around each point within $\mathbf{x_T}$. For any image point, $\mathbf{H}(\mathbf{x_T},\mathbf{x_{T+a_x}})$ represents a row of a sparse Hessian matrix $\mathbf{H}$ whose non-zero components are defined by $\mathbf{a_x}$. In other words, $\mathbf{a_x}$, which can be estimated as a function of the decrease in amplitude of the Hessian diagonal, defines the *filter-size* around each image point. Valenciano (2008) reviews the computational savings from this approximation. Throughout the rest of this paper, our discussions of the Hessian refer to the definition in equation 5. We use matrix-vetor notations to simplify the RJID methodology.

Least-squares inversion of time-lapse seismic data sets

We re-write the linear modeling operation in equation 1 as a convolution of an operator $\mathbf{L}$ with the earth reflectivity $\mathbf{m}$:

$$\mathbf{d} = \mathbf{L}\mathbf{m}. \quad (6)$$

Given two data sets (baseline and monitor), acquired over an evolving model at times $\mathbf{0}$ and $\mathbf{1}$ respectively, we can write

$$\begin{aligned} \mathbf{d}_0 &= \mathbf{L}_0\mathbf{m}_0, \\ \mathbf{d}_1 &= \mathbf{L}_1\mathbf{m}_1, \end{aligned} \quad (7)$$

where $\mathbf{m}_0$ and $\mathbf{m}_1$ are the baseline and monitor reflectivities and $\mathbf{d}_0$ and $\mathbf{d}_1$ are the data sets modeled by $\mathbf{L}_0$ and $\mathbf{L}_1$.

Applying the adjoint operators $\bar{\mathbf{L}}_0^T$ and $\bar{\mathbf{L}}_1^T$ to $\mathbf{d}_0$ and $\mathbf{d}_1$ respectively, we obtain the migrated baseline $\tilde{\mathbf{m}}_0$ and monitor $\tilde{\mathbf{m}}_1$ images:

$$\begin{aligned} \tilde{\mathbf{m}}_0 &= \bar{\mathbf{L}}_0^T\mathbf{d}_0, \\ \tilde{\mathbf{m}}_1 &= \bar{\mathbf{L}}_1^T\mathbf{d}_1, \end{aligned} \quad (8)$$

where $\bar{\mathbf{L}}_i^T$ denotes conjugate transpose of $\mathbf{L}_i$. The *raw* time-lapse image $\Delta\tilde{\mathbf{m}}$ is the difference between the migrated images:

$$\Delta\tilde{\mathbf{m}} = \tilde{\mathbf{m}}_1 - \tilde{\mathbf{m}}_0. \quad (9)$$

Because of non-repeatability caused by differences in acquisition geometries and other sources, $\tilde{\mathbf{m}}_\mathbf{0}$ and $\tilde{\mathbf{m}}_\mathbf{1}$ must be *cross-equalized* before $\Delta\tilde{\mathbf{m}}$ is computed. Previous authors (Rickett and Lumley, 2001; Calvert, 2005; Hall, 2006) have discussed a wide range of cross-equalization methods. The proposed method is an equalization method based on a linearized acoustic wave-equation modeling/imaging approximation.

Following the definitions in equation 2, we define two quadratic cost functions for the modeling experiments (equation 7):

$$\begin{aligned} S(\mathbf{m_0}) &= \|\mathbf{L}_0\mathbf{m}_0 - \mathbf{d}_0\|_2^2, \\ S(\mathbf{m_1}) &= \|\mathbf{L}_1\mathbf{m}_1 - \mathbf{d}_1\|_2^2, \end{aligned} \quad (10)$$

which when minimized give the solutions $\hat{\mathbf{m}}_\mathbf{0}$ and $\hat{\mathbf{m}}_\mathbf{1}$, where

$$\begin{aligned} \hat{\mathbf{m}}_0 &= (\bar{\mathbf{L}}_0^T\mathbf{L}_0)^\dagger\bar{\mathbf{L}}_0^T\mathbf{d}_0, \\ \hat{\mathbf{m}}_1 &= (\bar{\mathbf{L}}_1^T\mathbf{L}_1)^\dagger\bar{\mathbf{L}}_1^T\mathbf{d}_1, \end{aligned} \quad (11)$$

and $(\cdot)^\dagger$ denotes approximate inverse. Estimating $\hat{\mathbf{m}}_\mathbf{0}$ and/or $\hat{\mathbf{m}}_\mathbf{1}$ by minimizing equation 10 is the so-called *data-space* least-squares migration/inversion method. Substituting equation 8 and $\bar{\mathbf{L}}_0^T\mathbf{L}_0 = \mathbf{H}$ into equation 11, we write

$$\begin{aligned} \hat{\mathbf{m}}_0 &= \mathbf{H}_\mathbf{0}^\dagger\tilde{\mathbf{m}}_0, \\ \hat{\mathbf{m}}_1 &= \mathbf{H}_\mathbf{1}^\dagger\tilde{\mathbf{m}}_1. \end{aligned} \quad (12)$$

Because, in general, $\mathbf{H_0}$ and $\mathbf{H_1}$ cannot be directly inverted, equation 13 can be solved using iterative inverse filtering:

$$\begin{aligned} \mathbf{H}_0\hat{\mathbf{m}}_0 &= \tilde{\mathbf{m}}_0, \\ \mathbf{H}_1\hat{\mathbf{m}}_1 &= \tilde{\mathbf{m}}_1, \end{aligned} \quad (13)$$

which is the so-called *model-space* least-squares migration/inversion method. An inverted time-lapse image, $\Delta\hat{\mathbf{m}}$, can be obtained as difference between the two images, $\hat{\mathbf{m}}_0$ and $\hat{\mathbf{m}}_1$:

$$\Delta\hat{\mathbf{m}} = \hat{\mathbf{m}}_1 - \hat{\mathbf{m}}_0. \quad (14)$$

In this paper, we refer to the method of computing the time-lapse image using equation 14 as *separate inversion*.

Joint inversion for image differences

In order to solve a single joint inversion problem in which the baseline and time-lapse images are simultaneously estimated, we re-write equation 7 as

$$\begin{aligned} \mathbf{d}_0 &= \mathbf{L}_0\mathbf{m}_0, \\ \mathbf{d}_1 &= \mathbf{L}_1(\mathbf{m}_0 + \Delta\mathbf{m}), \end{aligned} \quad (15)$$

where $\mathbf{m}_0 + \Delta\mathbf{m} = \mathbf{m}_1$. Combining these expressions we have

$$\begin{bmatrix} \mathbf{d}_0 \\ \mathbf{d}_1 \end{bmatrix} = \begin{bmatrix} \mathbf{L}_0 & \mathbf{0} \\ \mathbf{L}_1 & \mathbf{L}_1 \end{bmatrix} \begin{bmatrix} \mathbf{m}_0 \\ \Delta\mathbf{m} \end{bmatrix}, \quad (16)$$

which can be solved by minimizing the cost function

$$S(\mathbf{m_0},\Delta\mathbf{m}) = \left\| \begin{bmatrix} \mathbf{L}_0 & \mathbf{0} \\ \mathbf{L}_1 & \mathbf{L}_1 \end{bmatrix} \begin{bmatrix} \mathbf{m}_0 \\ \Delta\mathbf{m} \end{bmatrix} - \begin{bmatrix} \mathbf{d}_0 \\ \mathbf{d}_1 \end{bmatrix} \right\|_2^2. \quad (17)$$

Direct minimization of equation 17 with an iterative solver is computationally expensive (number of iterations times six times cost of one migration). Because several iterations are usually required to reach a desirable solution, and because inversion is usually repeated several times to fine-tune parameters, the overall cost of this scheme makes it impractical. One advantage of the RJID method (discussed next) is that modifications can be made to inversion parameters and the inversion repeated several times without the need for migration or modeling (demigration) required in iterative least-squares *data-space* migration/inversion.

The least-squares solution to equation 16 is given by

$$\begin{bmatrix} \hat{\mathbf{m}}_0 \\ \Delta\hat{\mathbf{m}} \end{bmatrix} = \begin{bmatrix} \bar{\mathbf{L}}_0^T\mathbf{L}_0 + \bar{\mathbf{L}}_1^T\mathbf{L}_1 & \bar{\mathbf{L}}_1^T\mathbf{L}_1 \\ \bar{\mathbf{L}}_1^T\mathbf{L}_1 & \bar{\mathbf{L}}_1^T\mathbf{L}_1 \end{bmatrix}^{\dagger} \begin{bmatrix} \bar{\mathbf{L}}_0^T & \bar{\mathbf{L}}_1^T \\ \mathbf{0} & \bar{\mathbf{L}}_1^T \end{bmatrix} \begin{bmatrix} \mathbf{d}_0 \\ \mathbf{d}_1 \end{bmatrix}, \tag{18}$$

or

$$\begin{bmatrix} \hat{\mathbf{m}}_0 \\ \Delta\hat{\mathbf{m}} \end{bmatrix} = \begin{bmatrix} \mathbf{H}_0 + \mathbf{H}_1 & \mathbf{H}_1 \\ \mathbf{H}_1 & \mathbf{H}_1 \end{bmatrix}^{\dagger} \begin{bmatrix} \tilde{\mathbf{m}}_0 + \tilde{\mathbf{m}}_1 \\ \tilde{\mathbf{m}}_1 \end{bmatrix}, \tag{19}$$

where the inverted baseline $\hat{\mathbf{m}}_0$ and time-lapse $\Delta\hat{\mathbf{m}}$ images are obtained by solving the inverse filtering problem

$$\begin{bmatrix} \mathbf{H}_0 + \mathbf{H}_1 & \mathbf{H}_1 \\ \mathbf{H}_1 & \mathbf{H}_1 \end{bmatrix} \begin{bmatrix} \hat{\mathbf{m}}_0 \\ \Delta\hat{\mathbf{m}} \end{bmatrix} = \begin{bmatrix} \tilde{\mathbf{m}}_0 + \tilde{\mathbf{m}}_1 \\ \tilde{\mathbf{m}}_1 \end{bmatrix}. \tag{20}$$

Following the same procedure, similar systems of equations can be constructed for any number of data sets. For example, a three-survey system is given by

$$\begin{bmatrix} \mathbf{H_0} + \mathbf{H_1} + \mathbf{H_2} & \mathbf{H_1} + \mathbf{H_2} & \mathbf{H_2} \\ \mathbf{H_1} + \mathbf{H_2} & \mathbf{H_1} + \mathbf{H_2} & \mathbf{H_2} \\ \mathbf{H_2} & \mathbf{H_2} & \mathbf{H_2} \end{bmatrix} \begin{bmatrix} \hat{\mathbf{m}}_0 \\ \Delta\hat{\mathbf{m}}_1 \\ \Delta\hat{\mathbf{m}}_2 \end{bmatrix} = \begin{bmatrix} \tilde{\mathbf{m}}_0 + \tilde{\mathbf{m}}_1 + \tilde{\mathbf{m}}_2 \\ \tilde{\mathbf{m}}_1 + \tilde{\mathbf{m}}_2 \\ \tilde{\mathbf{m}}_2 \end{bmatrix}. \tag{21}$$

Note that it is unnecessary to explicitly form the Hessian operators in equations 20 and 21 because they are composed of simple combinations of $\mathbf{H_0}$ to $\mathbf{H_N}$ for N surveys. We have implemented these operators for any arbitrary number of surveys using sparse convolution operators.

Regularization

Because seismic inversion is ill-posed, model regularization is often required to ensure stability and convergence to a geologically consistent solution. For many seismic monitoring objectives, the known geology and reservoir architecture provide useful regularization information. As shown by Ayeni and Biondi (2008), equation 21 can be extended to include such prior information, to give

$$\left(\begin{bmatrix} \mathbf{H_0} + \mathbf{H_1} + \mathbf{H_2} & \mathbf{H_1} + \mathbf{H_2} & \mathbf{H_2} \\ \mathbf{H_1} + \mathbf{H_2} & \mathbf{H_1} + \mathbf{H_2} & \mathbf{H_2} \\ \mathbf{H_2} & \mathbf{H_2} & \mathbf{H_2} \end{bmatrix} + \begin{bmatrix} \mathbf{R_{00}} & \mathbf{0} & \mathbf{0} \\ \mathbf{0} & \mathbf{R_{11}} & \mathbf{0} \\ \mathbf{0} & \mathbf{0} & \mathbf{R_{22}} \end{bmatrix} + \begin{bmatrix} \Lambda_{\mathbf{00}} & -\Lambda_{\mathbf{01}} & \mathbf{0} \\ -\Lambda_{\mathbf{10}} & 2\Lambda_{\mathbf{11}} & -\Lambda_{\mathbf{12}} \\ \mathbf{0} & -\Lambda_{\mathbf{21}} & \Lambda_{\mathbf{22}} \end{bmatrix} \right) \begin{bmatrix} \hat{\mathbf{m}}_0 \\ \Delta\hat{\mathbf{m}}_1 \\ \Delta\hat{\mathbf{m}}_2 \end{bmatrix} = \begin{bmatrix} \tilde{\mathbf{m}}_0 + \tilde{\mathbf{m}}_1 + \tilde{\mathbf{m}}_2 \\ \tilde{\mathbf{m}}_1 + \tilde{\mathbf{m}}_2 \\ \tilde{\mathbf{m}}_2 \end{bmatrix}, \tag{22}$$

where,

$$\begin{aligned} \mathbf{R_{ij}} &= \varepsilon_\mathbf{i}\mathbf{R'}_\mathbf{i}\varepsilon_\mathbf{j}\mathbf{R_j} \\ \Lambda_{\mathbf{ij}} &= \zeta_\mathbf{i}\Lambda'_\mathbf{i}\zeta_\mathbf{j}\Lambda_\mathbf{j} \end{aligned}, \tag{23}$$

where $\mathbf{R_{ij}}$ and $\Lambda_{\mathbf{ij}}$ are the spatial and temporal regularization respectively. Note that $\mathbf{R_{ij}}$ and $\Lambda_{\mathbf{ij}}$ are not explicitly computed, but instead, the regularization operators $\mathbf{R_{i,j}}$ and $\Lambda_{\mathbf{i,j}}$ (and their adjoints) are applied at each inversion step. Parameters ε_i and ζ_i determine the relative strengths of the spatial and temporal regularization respectively.

Depending on the problem size, computational domain and the available a priori information, the spatial and temporal regularization operators can be applied over several dimensions (e.g., stacked-image, subsurface offset, subsurface scattering-angles, etc.). Ajo-Franklin et al. (2005), Ayeni and Biondi (2008) and Ayeni et al. (2009) discuss alternative joint inversion formulations and applications.

NUMERICAL EXAMPLE

In this example, using seismic data sets acquired with different geometries, we aim to image seismic amplitude changes at a reservoir located under a salt block (Figure 1). Using a variable-density acoustic finite-difference algorithm, we simulated four data sets at different stages of reservoir depletion. Each data set consists of 76 shots spaced at 80 m and 301 receivers spaced at 20 m. In order to simulate non-repeated acquisition geometries, we modeled all the data sets with spatially different geometries as summarized in Table 1.

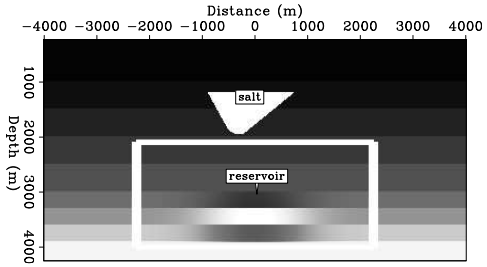

Figure 1: Synthetic impedance model. The salt velocity is 4500 m/s while the sediment velocity range from 2200 m/s to 2700 m/s. Densities range from 2.5 g/cc to 3.0 g/cc. The white box shows the target region and the expanding Gaussian anomaly centered at x = 0 m and z = 3500 m represents reservoir property change.

We migrated the data sets with a oneway wave-equation algorithm and computed the target-oriented Hessian matrices for the target region (Figure 1) using oneway Green's functions. No pre-processing applied to remove internal multiples from the data. For the inversion, the spatial and temporal regularization operators are gradients along reflector dips and leaky temporal derivatives respectively.

Table 1: Modeling parameters for synthetic data sets

	Shot/receiver depth	Shot/receiver spread
Geometry 1	0m	−3000 to 3000m
Geometry 2	100m	−3500 to 2500m
Geometry 3	200m	−2600 to 3400m
Geometry 4	40m	−2900 to 3100m

We approximate the *true* reflectivity with the derivative of the impedance models for each survey. The *true* reflectivity time-lapse images computed as the difference between the three monitor reflectivities and the baseline are shown in Figure 2(a). Figure 2(b) shows the time-lapse images obtained from the migrated images. Note the large noise-level caused by the geometry differences and uneven illumination. Figure 2(c) shows the time-lapse images from separate inversion (equation 14). Note the improved resolution relative to Figure 2(b) and the increase in artifacts. Figure 2(d) shows the time-lapse images obtained from RJID. Although the same spatial regularization strength was used to generate the inverted results (Figures 2(c) and 2(d)), recall that separate inversion contains no temporal constraints.

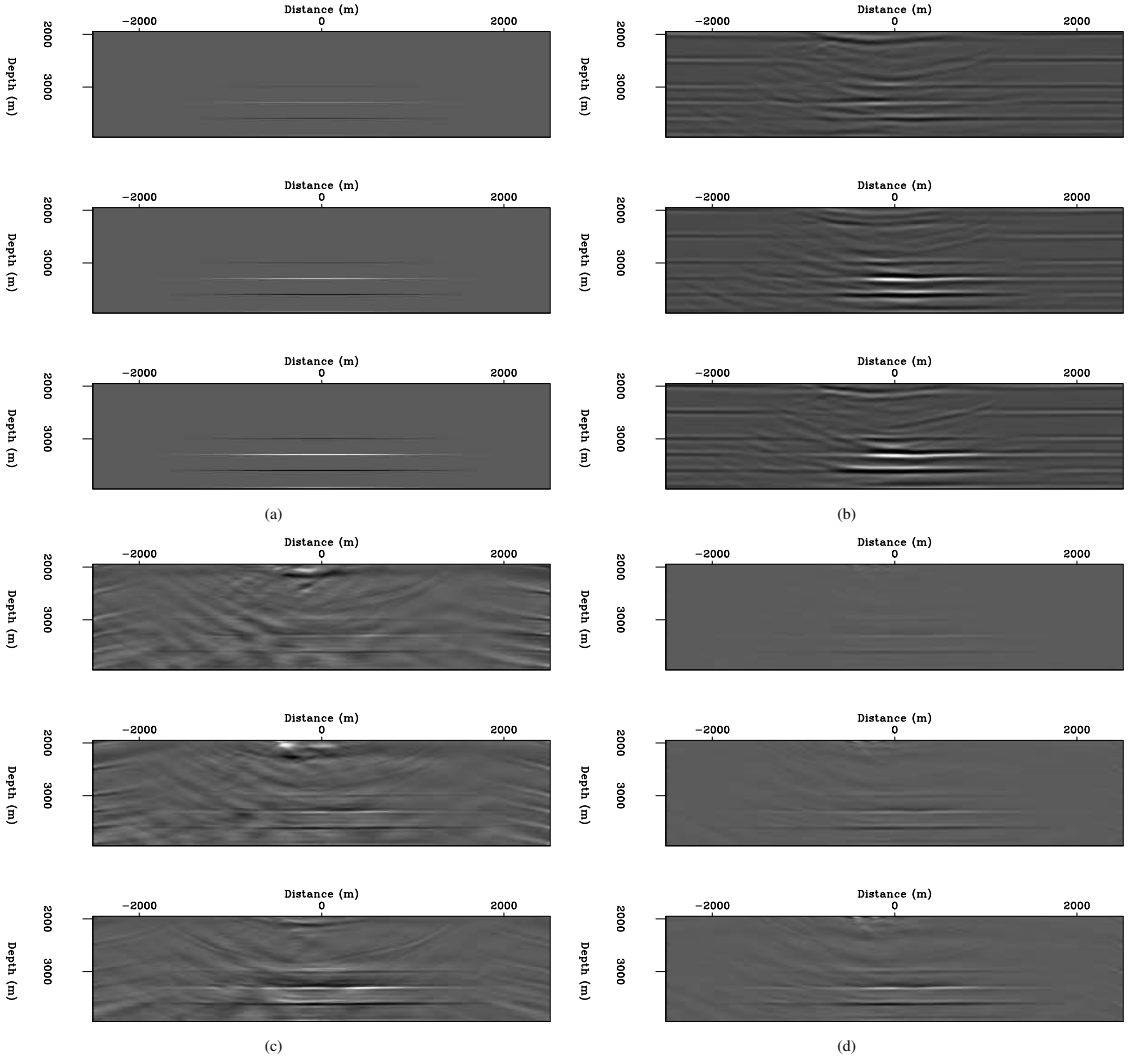

Figure 2: Cumulative time-lapse reflectivity changes at four different stages of production (with increasing change from top to bottom) from (a) the true reflectivity images, (b) migration, (c) separate inversion, and (d) joint inversion.

DISCUSSION AND CONCLUSIONS

We proposed a joint target-oriented wave-equation inversion method for imaging multiple time-lapse seismic data sets. The method, RJID, attenuates geometry and overburden artifacts which are not accounted for by the migration operator. RJID outputs an inverted baseline and time-lapse images.

From the numerical example, we see that overburden complexity and geometry differences degrade time-lapse images (Figure 2(b)). This degradation is expected because the migrated images (not shown) have uneven and different illumination throughout the target region. The Hessian matrices, which capture illumination and geometry information for each survey, show significant differences in diagonal and off-diagonal components. Because of the poor conditioning of the Hessian matrices, even with spatial regularization, time-lapse images obtained from separate inversion contain high amplitude residual artifacts (Figure 2(c)). The quality of the time-lapse images can be improved by using RJID (Figure 2(d)). The improvement derived from using RJID over separate inversion is a result of temporal constraints included in the RJID formulation. Because we used one-way operators in the example, the Hessian matrices contain no multiple information. Although RJID suppresses multiple artifacts (Figure 2(d)) relative to migration (Figure 2(b)) or separate inversion (Figure 2(c)), practical applications will require attenuation of multiples prior to inversion. From the results (Figure 2), we conclude that RJID provides a framework for obtaining good-quality, high-resolution time-lapse images from multiple seismic data sets.

ACKNOWLEDGMENTS

The authors thank sponsors of the Stanford Exploration Project for their financial support.

EDITED REFERENCES

Note: This reference list is a copy-edited version of the reference list submitted by the author. Reference lists for the 2009 SEG Technical Program Expanded Abstracts have been copy edited so that references provided with the online metadata for each paper will achieve a high degree of linking to cited sources that appear on the Web.

REFERENCES

Ajo-Franklin, J. B., J. Urban, and J. M. Harris, 2005, Temporal integration of seismic traveltime tomography: 75th Annual International Meeting, SEG, Expanded Abstracts, 2468–2471.

Ayeni, G., and B. Biondi, 2008, Joint wave-equation inversion of time-lapse seismic data: Stanford Exploration Project Report, **136**, 71–96.

Ayeni, G., Y. Tang, and B. Biondi, 2009, Preconditioned joint least-squares inversion of blended time-lapse seismic data sets: 79th Annual International Meeting, SEG, Expanded Abstracts, submitted.

Batzle, M., and Z. Wang, 1992, Seismic properties of pore fluids: Geophysics, **57**, 1396–1408.

Calvert, R., 2005, Insights and methods for 4D reservoir monitoring and characterization: SEG/EAGE DISC Distinguished Instructor Lecture Course.

Guitton, A., 2004, Amplitude and kinematic corrections of migrated images for nonunitary imaging operators: Geophysics, **69**, 1017–1024.

Hall, S. A., 2006, A methodology for 7d warping and deformation monitoring using time-lapse seismic data: Geophysics, **71**, no. 4, O21–O31.

Lefeuvre, F., Y. Kerdraon, J. Peliganga, S. Medina, P. Charrier, R. L'Houtellier, and D. Dubucq, 2003, Improved reservoir understanding through rapid and effective 4D: Girassol field, Angola, West Africa: 73rd Annual International Meeting, SEG, Expanded Abstracts, 1334–1337.

Plessix, R. -E., and W. Mulder, 2004, Frequency-domain finite-frequency amplitude-preserving migration: Geophysical Journal International, **157**, 975–985.

Rickett, J., 2003, Illumination-based normalization for wave-equation depth migration: Geophysics, **68**, 1371–1379.

Rickett, J. E., and D. E. Lumley, 2001, Cross-equalization data processing for time-lapse seismic reservoir monitoring: A case study from the Gulf of Mexico: Geophysics, **66**, 1015–1025.

Shin, C., S. Jang, and D.-J. Min, 2001, Improved amplitude preservation for prestack depth migration by inverse scattering theory: Geophysical Prospecting, **49**, 592–606.

Symes, W. W., 2008, Approximate linearized inversion by optimal scaling of prestack depth migration: Geophysics, **73**, no. 2, R23–R35.

Valenciano, A., 2008, Imaging by wave-equation inversion: Ph.D. thesis, Stanford University.

Whitcombe, D. N., J. M. Marsh, P. J. Clifford, M. Dyce, C. J. S. McKenzie, S. Campbell, A. J. Hill, R. S. Parr, C. Pearse, T. A. Ricketts, C. P. Slater, and O. L. Barkved, 2004, The systematic application of 4D in BP's North-West Europe operations — 5 years on: Approximate linearized inversion by optimal scaling of prestack depth migration. 2251–2254.

Zou, Y., L. R. Bentley, L. R. Lines, and D. Coombe, 2006, Integration of seismic methods with reservoir simulation, Pikes Peak heavy-oil field, Saskatchewan: The Leading Edge, **25**, 764–781.